Thinning down of thermal conductivity in ultrashort period superlattices

Iorwerth O. Thomas and G. P. Srivastava
School of Physics, University of Exeter, Stocker Road, Exeter EX4 4QL, United Kingdom
(Received 27 February 2013; revised manuscript received 3 July 2013; published 16 September 2013)

We present numerical results for the reduction of the lattice thermal conductivity tensor components $\{\kappa_{\alpha,\beta}\}$ in ultrashort period $(Si)_n(Ge)_n[001]$ superlattices, with $1 \leqslant n \leqslant 8$, where n represents the number of atomic bilayers. The calculations are made within the single-mode relaxation-time approximation, accounting for interatomic bond length relaxation and employing phonon dispersion relations obtained from density functional perturbation theory, a model anharmonic Hamiltonian to deal with three-phonon interactions involving acoustic as well as optical phonons in a two-material superlattice structure, and an improved scheme for phonon scattering due to mass smudging at interfaces. The cross-plane component of the conductivity is around 4.1 times smaller than the in-plane component for the $n = 8$ case at room temperature and an interface mass mixing (IMS) scattering strength of 0.05. Both the in-plane and cross-plane components of the conductivity decrease sharply with the superlattice period when the strength of the IMS scattering is kept constant. Incorporating physical considerations into the behavior of the IMS scattering, we predict a minimum of the thermal conductivity for $n \approx 4$. We estimate that a small amount of interface mass smudging results in a reduction of around 3%–14% in the zz conductivity component for temperatures of 100 to 700 K when boundary scattering is relatively weak. We estimate relevant phonon scattering rates to explain available experimental conductivity measurements on a system comparable in size to the (8,8) superlattice.

DOI: 10.1103/PhysRevB.88.115207 PACS number(s): 63.22.Np, 63.20.dk, 65.80.−g

I. INTRODUCTION

The recent renaissance of interest in the thermoelectric effect has been driven by the prospect of a dramatic increase in the efficiency of thermoelectric conversion in various compounds through nanostructuring,[1,2] an improvement which would entail that such thermoelectric materials would now be eminently suitable for industrial applications. Much of the discussion centers around which components of the dimensionless figure of merit function ZT should be enhanced or reduced in order to best increase the efficiency of nanostructured systems. It is generally agreed that reducing the lattice contribution to the total thermal conductivity ($\kappa_{\rm ph}$) of the system is a promising direction in this respect.

Over the past 50 years, the most routinely employed theoretical approach for the calculation of the lattice thermal conductivity has been the single-mode relaxation-time method, based on the Boltzmann transport theory and evaluated within the isotropic continuum scheme (see Ref. 3 and references therein). This and other methods have successfully been applied to explain results for bulk insulators and semiconductors, but they generally require the use of several adjustable parameters in expressing the phonon anharmonic relaxation rates (see, e.g., the discussion presented in Ref. 4). Such schemes lack predictive power and are incapable of providing numerically trustworthy results for nanostructured materials. This limitation arises for several reasons: (i) the large unit cells required to treat nanostructured materials result in many phonon branches, with many exhibiting anisotropic dispersion relations that can be significantly different from bulk results, (ii) atomic vibrations are phase correlated within a repeat period in composite systems such as superlattices where more than one material is present in an ordered fashion, and (iii) even if the most careful growth techniques are employed, some level of mass mixing at the interfaces between materials in these ordered composite nanostructures is inevitable. A combination of these factors alters the phonon group velocity and phonon lifetime, and hence will significantly change the thermal conductivity of composite structures when compared to individual materials. In recent years, a number of research groups have endeavored to describe the phonon thermal conductivity through first-principles calculations of phonon dispersion relations and anharmonic force constants in bulk and nanostructured solids.[5–7] However, these approaches are not yet fully mature. In addition, first-principles approaches are not yet able to include the temperature dependence of the anharmonic force constants, which are important for the explanation of the thermal conductivity at high temperatures.

Our group has adopted an intermediate-level approach, in which phonon dispersion relations are computed using a first-principles approach and the anharmonic crystal potential is expressed in the spirit of the continuum scheme, allowing for temperature dependence of anharmonic scattering strength.[8–11] In this work, we extend our recent attempt to study $\kappa_{\rm ph}$ in ultrathin SiGe superlattice (SL) systems,[8,9,11] incorporating interatomic bond length relaxation and including the effects of all relevant scattering effects. In order to achieve this, we use a model anharmonic Hamiltonian that describes three-phonon interactions involving optical as well as acoustic phonons in superlattice structures. The proposed Hamiltonian is a revised version of that presented in our earlier works.[10,11] We also present an improved scheme that accounts for phonon scattering arising from interface mass mixing in such structures. Using these features and phonon dispersion relations obtained from density functional perturbation theory, we present numerical results on the reduction of the lattice thermal conductivity in ultrashort period SiGe superlattices.

Before we proceed, we should first clarify our notation. We will be examining SLs of the form $(Si)_n(Ge)_m[001]$. The value of n or m indicates the number of Si or Ge *bilayers* that a given Si or Ge layer contains; we will sometimes denote a

SL as a (m,n) superlattice, or SL(n, m), and we take $n = m$ throughout this work. When we speak in terms of Cartesian axes, we take z to be the growth or cross ([001]) direction and the in-plane or planar x and y directions to be [110] and [1$\bar{1}$0], respectively. We estimate relevant phonon scattering rates to explain the experimental conductivity measurements by Borca-Tascuic *et al.*[12] on a system comparable in size to the (8,8) superlattice.

II. THEORETICAL DISCUSSION

A. Thermal conductivity tensor

We calculate the elements of the lattice thermal conductivity tensor $\kappa_{\rm ph}$ using the single-mode relaxation-time approximation[3,13]

$$\kappa_{\mu\nu} = \frac{\hbar^2}{N_0 \Omega k_{\rm B} T^2} \sum_{\boldsymbol{q}s} \omega^2(\boldsymbol{q}s) c_{s,\mu}(\boldsymbol{q}) c_{s,\nu}(\boldsymbol{q}) \tau(\boldsymbol{q}s) \bar{n}_{\boldsymbol{q}s}(\bar{n}_{\boldsymbol{q}s} + 1). \tag{1}$$

Here, N_0 is the number of unit cells, Ω is the volume of a unit cell, and $\omega(\boldsymbol{q}s)$ and $c_{s,\mu}(\boldsymbol{q})$ are, respectively, the frequency and the velocity component in the μth direction of the phonon mode labeled by $(\boldsymbol{q}s)$, with $\boldsymbol{q}$ as the wave vector and s the branch label, $\bar{n}_{\boldsymbol{q}s}$ is the equilibrium Bose-Einstein distribution for that mode, and $\tau(\boldsymbol{q}s)$ is the relaxation time of phonons in their single modes $\{\boldsymbol{q}s\}$. It is clear from the above equation that numerically accurate estimates of three important quantities are required for the calculation of the conductivity tensor. These are phonon dispersion relations, velocity components, and the total relaxation time for a given makeup of the superlattice.

The total relaxation time $\tau(\boldsymbol{q}s)$ depends on various scattering processes as follows:

$$\begin{aligned}\tau^{-1}(\boldsymbol{q}s) = {} & \tau_{\rm LB}^{-1}(\boldsymbol{q}s) + \tau_{\rm MD}^{-1}(\boldsymbol{q}s) + \tau_{\rm AL}^{-1}(\boldsymbol{q}s) + \tau_{\text{el-ph}}^{-1}(\boldsymbol{q}s) \\ & + \tau_{\rm IMS}^{-1}(\boldsymbol{q}s) + \tau_{\rm IDS}^{-1}(\boldsymbol{q}s) + \tau_{\rm AH}^{-1}(\boldsymbol{q}s).\end{aligned} \tag{2}$$

Here, the contributions to the relaxation time are boundary scattering [$\tau_{\rm LB}(\boldsymbol{q}s)$], isotopic and other point-mass-defect scattering [$\tau_{\rm MD}(\boldsymbol{q}s)$], alloy scattering [$\tau_{\rm AL}(\boldsymbol{q}s)$], electron-phonon scattering [$\tau_{\text{el-ph}}(\boldsymbol{q}s)$], interface mass mixing scattering (IMS) [$\tau_{\rm IMS}(\boldsymbol{q}s)$], interface defect scattering (IDS) [$\tau_{\rm IDS}(\boldsymbol{q}s)$], and anharmonic scattering [$\tau_{\rm AH}(\boldsymbol{q}s)$].

In this work, we restrict ourselves to undoped ultrathin $(\text{Si})_n(\text{Ge})_n$[001] SLs, with $1 \leqslant n \leqslant 8$, entailing that we can neglect the contribution $\tau_{\text{el-ph}}^{-1}(\boldsymbol{q}s)$. The alloy scattering is included only for SL (1,1), which is treated as a Si(50%)-Ge(50%) alloy. For SLs with $n > 1$, we do not allow full alloy scattering, but instead only the appropriate degree of isotope and other point-defect scattering in each layer. The term $\tau_{\rm IDS}^{-1}(\boldsymbol{q}s)$ can be thought of as arising from several sources: point defects at or near Si-Ge interfaces, interface strain resulting from lattice mismatch between Si and Ge, and the development of interface dislocations in thick Si-Ge superlattices.[14,15] The first two contributions can be expected to depend on the phonon mode in the same manner as is expected for the point-defect contribution $\tau_{\rm MD}^{-1}(\boldsymbol{q}s)$ and so are absorbed into it. The second contribution will be ignored, as dislocations are not expected to develop for the ultrathin SLs considered in this work, whose layer thicknesses are below the critical thickness (equivalent to $n \approx 10$).[14,15] Our treatment of boundary scattering, point-mass-defect scattering, and alloy scattering is the same as described in an earlier publication.[10] In that work, it was concluded that in order to successfully explain the conductivity of a Si-Ge alloy, an increased strength of the combined mass-defect and alloy scattering is required. In what follows, we will discuss phonon scattering mechanisms which rely on the formation of a superlattice.

B. Phonon scattering due to mass mixing across interfaces (IMS)

In previous works, we formulated the phonon scattering due to mass mixing across interfaces (IMS) by considering a periodic unreconstructed superlattice $A(m)/B(n)$ with m layers of material A and n layers of material B.[8,9] However, in this work we adopt a revised scheme for the probability of a given layer mixing. We express the phonon relaxation rate as

$$\tau_{\rm IMS}^{-1}(\boldsymbol{q}s) = \frac{\pi \Gamma_{\rm IMS}}{6N_0} \sum_{\boldsymbol{q}s} \omega(\boldsymbol{q}s)\omega(\boldsymbol{q}'s')\delta[\omega(\boldsymbol{q}s) - \omega(\boldsymbol{q}'s')] \frac{(\bar{n}_{\boldsymbol{q}'s'} + 1)}{(\bar{n}_{\boldsymbol{q}s} + 1)}, \tag{3}$$

where

$$\Gamma_{\rm IMS} = \mathcal{P}\left(\frac{\Delta M}{M}\right)^2 \left(\left[1 - \frac{e_A e'_A}{e_B e'_B}\right]^2 + \left[1 - \frac{e_B e'_B}{e_A e'_A}\right]^2 \right). \tag{4}$$

Here, $M = (mM_A + nM_B)$ and $\Delta M = |M_A - M_B|$. Following Refs. 8 and 9 we use the solution of the one-dimensional diatomic linear chain model (along the superlattice growth direction) to determine the ratio of the amplitudes of the eigenvectors e_A and e_B:

$$\frac{e_B}{e_A} = \frac{\left[\frac{1}{M_0} - \Delta\left(\frac{1}{M}\right)\right]\cos(l_z q_z)}{\left[\left(\frac{1}{M_0}\right)^2 + \left\{\Delta\left(\frac{1}{M}\right)\right\}^2 \sin^2(l_z q_z)\right]^{1/2} - \Delta\left(\frac{1}{M}\right)}, \tag{5}$$

where l_z is the superlattice period in the z direction, $M_0 = (M_A^{-1} + M_B^{-1})/2$, and $\Delta(1/M) = (M_A^{-1} - M_B^{-1})/2$. We describe our scheme for determining $\mathcal{P}$ in Appendix A, and provide further discussion on its choice in a later section.

C. Phonon anharmonic scattering rate

Following the basic theory presented in the book by Ziman[16] (and references therein), in earlier publications (see, e.g., Refs. 3 and 17) we have developed an expression for the cubic anharmonicity in an elastic continuum. This has been successfully employed in treating three-phonon interactions in bulk materials, but only when describing acoustic phonons participating in processes of the type ac + ac $\leftrightarrow$ ac. In our recent publications,[8–10] we developed a revised version of the anharmonic Hamiltonian for bulk materials that can include all allowed three-phonon processes involving optical as well as acoustic modes. The basic physical considerations behind that approach are rooted in the theory advocated by Klemens[18] and Ridley and Gupta.[19] In this work, we use a version of the anharmonic Hamiltonian that accounts for the presence of two material species in a superlattice structure of the type A/B, made of alternating layers of materials A and B. Following

the discussions in Refs. 9–11 and 20 and in Appendix B, we express the anharmonic phonon relaxation rate in such a superlattice structure in the form

$$\tau_{\rm AH}^{-1}(\boldsymbol{q}s) = \frac{\pi\hbar\bar{\gamma}^2}{\rho N_0 \Omega \bar{c}^2} \sum_{\boldsymbol{q}'s',\,\boldsymbol{q}''s'',\,\boldsymbol{G}} \frac{(\mathcal{R}_{\boldsymbol{q}s,\,\boldsymbol{q}'s',\,\boldsymbol{q}''s''})^2}{\omega(\boldsymbol{q}s)\omega(\boldsymbol{q}'s')\omega(\boldsymbol{q}''s'')} \times \mathcal{D}(\boldsymbol{q},\boldsymbol{q}',\boldsymbol{q}'') \Bigg[\frac{\bar{n}_{\boldsymbol{q}'s'}(\bar{n}_{\boldsymbol{q}''s''}+1)}{(\bar{n}_{\boldsymbol{q}s}+1)} \delta[\omega(\boldsymbol{q}s)+\omega(\boldsymbol{q}'s') - \omega(\boldsymbol{q}''s'')]\delta_{\boldsymbol{q}+\boldsymbol{q}',\,\boldsymbol{q}''+\boldsymbol{G}} + \frac{1}{2}\frac{\bar{n}_{\boldsymbol{q}'s'}\bar{n}_{\boldsymbol{q}''s''}}{\bar{n}_{\boldsymbol{q}s}} \times \delta[\omega(\boldsymbol{q}s)-\omega(\boldsymbol{q}'s')-\omega(\boldsymbol{q}''s'')]\delta_{\boldsymbol{q}+\boldsymbol{G},\,\boldsymbol{q}'+\boldsymbol{q}''} \Bigg], \quad (6)$$

where ρ is the average mass density in the superlattice structure, $\boldsymbol{G}$ is a reciprocal lattice vector, $\bar{c}$ is the long-wavelength acoustic phonon speed, and $\bar{\gamma}$ is the mode average of the *rescaled* Grüneissen constant (as defined in the Appendix of Ref. 10). The term $\mathcal{R}$ can be expressed as

$$\mathcal{R} = \bar{c}^2 \mathcal{B}^{\rm modified}_{i,j,k} = [\sqrt{\omega(i)\omega(j)}[\omega(i)+\omega(j)]|\omega_\Gamma(k)-\omega(k)| + \text{ similar terms with } i,\ j, \text{ and } k \text{ interchanged}]/3!, \quad (7)$$

as discussed in Appendix B. The *dual-mass term* $\mathcal{D}(\boldsymbol{q},\boldsymbol{q}',\boldsymbol{q}'')$ arises from the composite nature of the superlattice (i.e., presence of materials A and B). This term is interlinked with the onset of *mini-umklapp* anharmonic processes[20] governed by additional reciprocal translation vectors that are generated upon the formation of the superlattice periodicity. The following simple analytical expression for this term along the A/B superlattice growth direction can be obtained by considering the diatomic linear chain model:[20]

$$\mathcal{D}(\boldsymbol{q},\boldsymbol{q}',\boldsymbol{q}'') = \frac{1}{64}\left(\frac{\mathcal{A}_{AB}}{2\rho_A^{3/2}} + \frac{\mathcal{A}_{BA}}{2\rho_B^{3/2}}\right)^2 \quad (8)$$

with $\rho_{A(B)}$ being the density of material $A(B)$ and

$$\mathcal{A}_{ij} = 1 + \frac{\rho_i^{1/2}}{\rho_j^{1/2}}\left(\frac{e_j}{e_i}+\frac{e'_j}{e'_i}+\frac{e''_j}{e''_i}\right) + \frac{\rho_i}{\rho_j}\left(\frac{e_j e'_j}{e_i e'_i}+\frac{e'_j e''_j}{e'_i e''_i}+\frac{e_j e''_j}{e_i e''_i}\right) + \frac{\rho_i^{3/2}}{\rho_j^{3/2}}\left(\frac{e_j e'_j e''_j}{e_i e'_i e''_i}\right), \quad (9)$$

e_A and e_B being the vibrational eigenvectors in segments A and B, respectively.

It could be argued that all required phonon harmonic eigensolutions (viz., ω, and e_A and e_B) of the system may be obtained from *ab initio* calculations. While that is true in principle, we used the simple analytical expression in Eq. (5) for the ratio of the eigenvectors e_A and e_B and the above analytical descriptions of $\tau_{\rm AH}^{-1}(\boldsymbol{q}s)$ so as to ensure that calculations were both tractable and physically transparent. Our adoption of this manner of approach is defended in more detail in Ref. 10.

III. COMPUTATIONAL CONSIDERATIONS AND CHOICE OF PARAMETERS

A. Computational details

As per Ref. 11, relaxed interatomic bond lengths and the lattice constant in the superlattice structures $(\mathrm{Si})_n(\mathrm{Ge})_n[001]$ where $1 \leqslant n \leqslant 8$ were determined by using the total energy and force methods. The phonon eigensolutions for the superlattice structures were generated using the density functional perturbation theory components of the QUANTUM ESPRESSO package,[21] utilizing the local density approximation and norm-conserving pseudopotentials,[22] a lattice constant of $a_o = 5.54$ Å, and a plane-wave basis up to the kinetic energy cutoff of 15 Ry. Brillouin-zone summations required for the electronic (phonon) part of the calculations were performed with $10 \times 10 \times 2$ shifted (unshifted) Monkhorst-Pack (MP) grids.[23] From the resulting interatomic force constants, we generated phonon eigensolutions on a finer unshifted MP grid $16 \times 16 \times 12$ for all superlattices, in order to ensure a reasonable convergence of $\kappa_{\rm ph}$.

Phonon velocity components were computed using the finite difference method: $c_{s,\mu} = [\omega(\{\boldsymbol{q}+\Delta\boldsymbol{q}\}s)+\omega(\{\boldsymbol{q}-\Delta\boldsymbol{q}\}s)]/2\Delta q_\mu$, with $\Delta\boldsymbol{q}$ considered typically as $0.05\boldsymbol{q}$. We approximated the momentum conservation conditions in Eq. (6) by using suitable cutoffs for phonon wave-vector components along the x, y, and z directions and the Dirac delta functions governing energy conservation in Eqs. (3) and (6) were replaced by Gaussian functions, as described in Ref. 10. The parameter σ which controls the spread of the Gaussian function was selected so that test phonon density of states data produced by our thermal conductivity code approximated the features of the phonon density of states plot produced through using post-processing routines in the QUANTUM ESPRESSO package. Brillouin-zone summations required for the relaxation times and the thermal conductivity were carried out using the shifted $16 \times 16 \times 12$ MP grids.

We checked the convergence of the components of $\kappa(\equiv\kappa_{\rm ph})$ on $11 \times 11 \times 8$, $14 \times 14 \times 10$, $16 \times 16 \times 12$, and $20 \times 20 \times 14$ grids for (n,n) SLs, with $n = 1$ and 2, at $T = 300$ and 1000 K for a mass-defect scaling $P = 4.5$, $\bar{\gamma}$ as described in the subsequent section, $L_B = 4.4$ mm, and $\mathcal{P} = 0.05$ for $n = 2$ (there is no IMS scattering for $n = 1$). The worst (best) convergence when moving from $11 \times 11 \times 8$ to $14 \times 14 \times 10$ was 127% (60%) for the $n = 1$ (2) κ_{yy} (κ_{xx}) component at 1000 K (300 K), for $14 \times 14 \times 10$ to $16 \times 16 \times 12$ 37% (5%) for the $n = 2$ (1) κ_{zz} (κ_{zz}) component at 300 K, and for $16 \times 16 \times 12$ to $20 \times 20 \times 14$ 62% (32%) for the $n = 2$ (1) κ_{zz} (κ_{xx}) component at 1000 K. (Percentages are determined relative to the smallest value.) This suggests either that the components of κ converge in an oscillatory fashion, or that some numerical instability has set in for the finest grid size; alas, we lack the computational resources to ascertain which is the case. We therefore chose the $16 \times 16 \times 12$ grid as the best available. It should be noted that these are something of a worst-case example; similar calculations carried out at $L_B = 3.0 \times 10^{-7}$ m showed a similar trend as we increased the density of q points, however, the percentage difference between the results of subsequent q grids was much smaller (e.g., for the $16 \times 16 \times 12$ to $20 \times 20 \times 14$ shift, the worst values are 31% for $n = 1$ and 10% for $n = 2$ in both in-plane directions at 1000 K).

B. Selection of semiempirical anharmonic scattering parameters

When dealing with three-phonon umklapp (U) processes, we should consider complete shells of reciprocal translation vectors $\boldsymbol{G}$. For bulk Si and Ge, there are eight such vectors of magnitude $\sqrt{3}$ and six further vectors of magnitude 2 in units of $2\pi/a_0$, where a_0 is the cubic lattice constant. Considering only the first shell of eight vectors is usually sufficient for a satisfactory evaluation of the three-phonon umklapp relaxation rate; the addition of the second shell, containing six vectors, is more than adequate. To ensure that the U processes are well accounted for, we thus included all $\boldsymbol{G}$ vectors up to the magnitude of $2 \times (2\pi/a_0)$ for all the superlattice structures considered in this work. This results in 20 vectors for SL (1,1) and 28 vectors for SL (n,n), $n \geqslant 2$.

As mentioned above, our theory of the cubic crystal Hamiltonian (and thus of the anharmonic phonon relaxation time) is based on a reasonable choice of the long-wavelength limit of the rescaled Grüneisen constant $\bar{\gamma}$ for the superlattice structure. We observe that the choice of $\bar{\gamma}$ in the present version of the theory will be different from the choice made in our previous works, due to the use of $\mathcal{B}^{\text{modified}}_{i,j,k}$ in the present theory rather than the $\mathcal{B}_{i,j,k}$ used in our previous works (see Appendix B). There are two factors that need to be kept in mind when selecting a value of $\bar{\gamma}$ for the thermal conductivity calculations. One is that a choice must be made that can be related to the values for bulk Si and Ge materials. The second is that as the mode average of the Grüneisen constant γ is highly temperature dependent for bulk Si and Ge,[24,25] we should expect the same for the Si/Ge superlattices. At low temperatures, γ usually shows an increase with T.[26] Test calculations at temperature above 150 K for the (1,1) SL indicated that the following temperature-dependent form of $\bar{\gamma}$ is a reasonable choice:

$$\bar{\gamma} = \begin{cases} \gamma_0, & T < T_c \\ \gamma_0\left(1 + \frac{(T-T_c)}{T_c}\right)^{n_\gamma}, & T \geqslant T_c \end{cases} \tag{10}$$

with $\gamma_0 = 0.45$, $n_\gamma = 0.56$, and $T_c = 150$ K. The choice of these parameters produces values of $\bar{\gamma}$ that lie intermediate to values obtained experimentally for bulk Si and Ge, and close to the value for SiGe alloys in the temperature range 150–300 K.[25]

C. Modeling $\mathcal{P}(n)$, the interface mass-mixing probability factor

Interface mass smudging is an unavoidable reality which is usually unpredictable and dependent on superlattice growth conditions. Thus, theoretical investigations of phonon-interface scattering must be made by modeling $\mathcal{P}(n)$, the interface mass-mixing probability factor, in a physically reasonable manner. Note that $\mathcal{P}$ is the overall probability that *some* Si bilayer exchanges with a Ge bilayer.

We shall examine the effects of a constant value of $\mathcal{P}(n) = 0.05$, but we shall also consider the effects of allowing it to vary with n. What does this variation mean in physical terms? Let us assume a set of superlattices of various n, that are identical in all ways other than those which we explicitly mention. Let us assume that interface mixing occurs only between a fixed number of bilayers or monolayers that lie immediately on either side of each Si-Ge interface, and that the proportion of mixing across each interface is identical (as is the case in Refs. 8 and 9 and seems to be the case in the DFPT calculation of Ref. 7). We will constrain ourselves to a single cell of such a system, where there are two interfaces and so the total proportion of mixing on either side of an interface per cell is twice that of the proportion per interface. The overall probability $\mathcal{P}$ of *some* Si bilayer exchanges with a Ge bilayer must scale with the inverse of n because, as we increase n, we keep both the number of bilayers undergoing exchange fixed and the proportion of mixing in those bilayers the same, but the number of bilayers which are not permitted to undergo interchange increases. Essentially, while the proportion of bilayers adjacent to the interface undergoing exchange does not change with n, the overall proportion of layers undergoing exchange must decrease as the number of bilayers has increased, meaning that $\mathcal{P} \propto (n - 2 + B)^{-1}$ (for $n = 2$ has no bilayers where mixing does not occur, and B is a constant set to unity so that $\mathcal{P}$ is equal to twice the proportion of exchange at that thickness.)

In order to examine the effect of a simple form of variation of $\mathcal{P}$ on κ_{zz}, we shall consider the following forms of $\mathcal{P}$, inspired by the proportion of mixing in the interface-adjacent layers of Landry and McGaughey's[27] molecular dynamics calculation:

$$\mathcal{P}_A = \frac{0.24}{n-1}, \quad \mathcal{P}_B = \frac{0.48}{n-1}. \tag{11}$$

Here, $\mathcal{P}$ falls off in a fashion proportional to the number of bilayers separating the interface. $\mathcal{P}_A$ corresponds to a mixing proportion of 0.12 per interface; this is probably an underestimate since Ref. 27 makes use of a slightly more complicated IMS distribution and so we provide an upper bound on its effect through using $\mathcal{P}_B$, which assumes a mixing proportion of 0.24 per interface.

The assumption that only interface-adjacent bilayers may undergo mass mixing is questionable, and so some method of deriving $\mathcal{P}$ from a more general underlying distribution is desirable. One can, for example, choose a purely empirical distribution (as in Ref. 27), but in what follows we shall mostly be interested in a more theoretical account.

The full details of our model are provided in Appendix A, but we shall summarize the basic ideas here for clarity: we take each Si bilayer in the unit cell to have a probability of exchanging itself with a given Ge bilayer that is inversely proportional to the distance between them, and this probability is taken as giving the proportion of such exchanges that occur in a given sample. The rate of the falloff of this probability with distance is controlled by α (larger α entails a faster falloff), and the probability of exchange between two adjacent bilayers is controlled by B (a smaller B means a larger probability of exchange); we fix $B = 1$ in what follows. From this, we may calculate an overall value of $\mathcal{P}$ which can be used. We shall examine the effects of a "soft" decay of this probability characterized by $\alpha = 2.0$ and a "hard" decay characterized by a choice of $\alpha = 5.0$. The values of $\mathcal{P}$ for each n and the probability that a given bilayer in one half of the SL might exchange with any other bilayer in the other half are plotted in Fig. 1. For both parameter choices, we can see from the plots of the exchange probability against bilayer number (1 being the bilayer closest to the leftmost interface, n being that

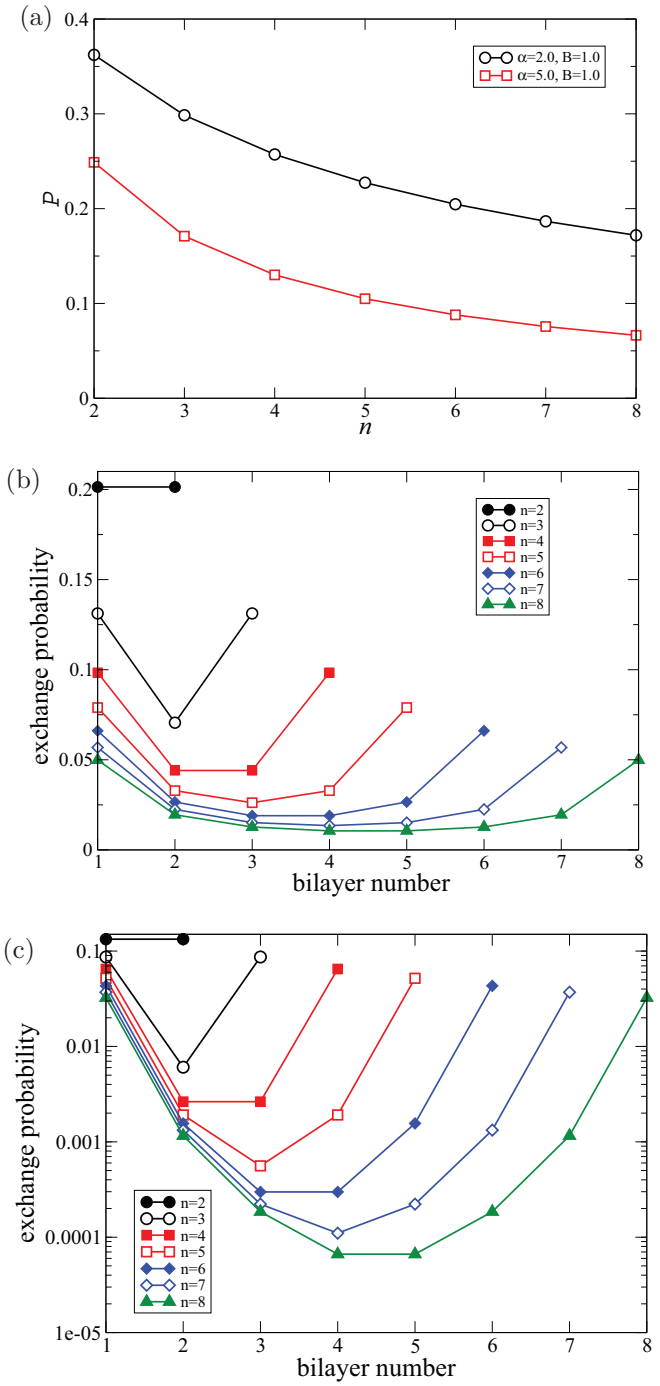

FIG. 1. (Color online) Variation in the probability $\mathcal{P}$ that a given Si(Ge) bilayer will exchange with a Ge(Si) bilayer: (a) with the number of bilayers n of each species within a superlattice unit cell, (b) for the parameters $\alpha = 2.0$, $B = 1.0$ and (c) for $\alpha = 5.0$, $B = 1.0$.

closest to the rightmost interface) that mass mixing is most pronounced in the interface layers; however, for the $\alpha = 5.0$ case, the exchange probability drops off rapidly as one moves further away from an interface, becoming almost negligible for the central layers of the larger lattices. This is not the case for $\alpha = 2.0$; here, there remains an appreciable probability of mixing even in the central layers of the larger superlattices. The upshot of these differences may be seen in Fig. 1(a); here we see that $\mathcal{P}$ is always larger for the $\alpha = 2.0$ case, as we would expect since it indicates a worse quality of interface.

IV. RESULTS AND DISCUSSION

A. Atomic relaxation, phonon dispersion curves, and phonon velocity

First, we shall summarize some relevant results concerning atomic relaxation and its effect on the phonon dispersions of ultrathin SLs presented in a previous study.[11] The numerical values of the cubic lattice constant and the interatomic bond length resulting from total-energy minimization and force reduction are $a_0 = 5.64$ Å, d(Si-Si) = 2.38–2.37 Å, d(Ge-Ge) = 2.42–2.43 Å, and d(Si-Ge) = 2.40 Å. These values are in agreement with well-known results (Vegard's law for the lattice constant; retention of Si-Si and Ge-Ge bond lengths close to their bulk values; Si-Ge bond length being close to the weighted average of individual bond lengths), and are discussed in more detail in Ref. 11.

The phonon dispersion of a superlattice structure is generally characterized by three features: zone folding (due to periodicity larger than in bulk structure), the formation of minigaps in the spectrum, and the confinement (or reduction in dispersion) of branches. While the magnitudes of minigaps generally decrease, the degree of confinement increases as the superlattice periodicity (equivalently, the superlattice index n) is increased. The enlargement of periodicity along the growth direction also causes the above characteristics to be present to some extent in the planar directions. These features can be clearly seen from a comparison of results presented in Fig. 2 for SL (1,1) and SL (4,4). The most significant changes in the phonon dispersion curves and density of states are noted for frequencies above 200 cm^{-1}. For all the SLs studied, the effect of relaxed atomic geometry is to shift the maximum frequency upwards. While the general qualitative structure of the density of states remains unaffected, most of the peaks above 200 cm^{-1} are shifted upwards. A more detailed examination of the effects of atomic relaxation on this and other phonon-related properties of superlattices may be found in Ref. 11.

Our computed average phonon speeds for the acoustic branches (calculated at the MP grid point closest to Γ) are $\bar{c}$(acoustic) = 6078, 3614, (4633, 4753, 4821, 5035, 5000) ms^{-1} for Si bulk, Ge bulk, and SL structures with n = 1–5. The corresponding values when averaged over all phonon branches and q points are c(all branch and momenta average) = 3349, 2011, (2855, 2830, 2922, 3223, 3239) ms^{-1} for Si bulk, Ge bulk, and SL structures with n = 1–5, respectively.

B. Results for the (1,1) and (8,8) Sls

Figure 3 presents the results of our calculations of the lattice thermal conductivity tensor components for the (1,1) and (8,8) superlattices. We provide some discussion on the tensor nature of the conductivity for both SLs. We also attempt to compare our results for κ_{zz} for the (8,8) SL with measurements made on a SiGe[001] superlattice of a similar repeat period. In Fig. 3(a), we present and discuss our phonon conductivity results along the growth direction κ_{zz} for the (1,1) SL. We considered an effective average sample size $L_B = 4.4 \times 10^{-3}$ m (equivalent to the sample size in the bulk measurements by Glassbrenner

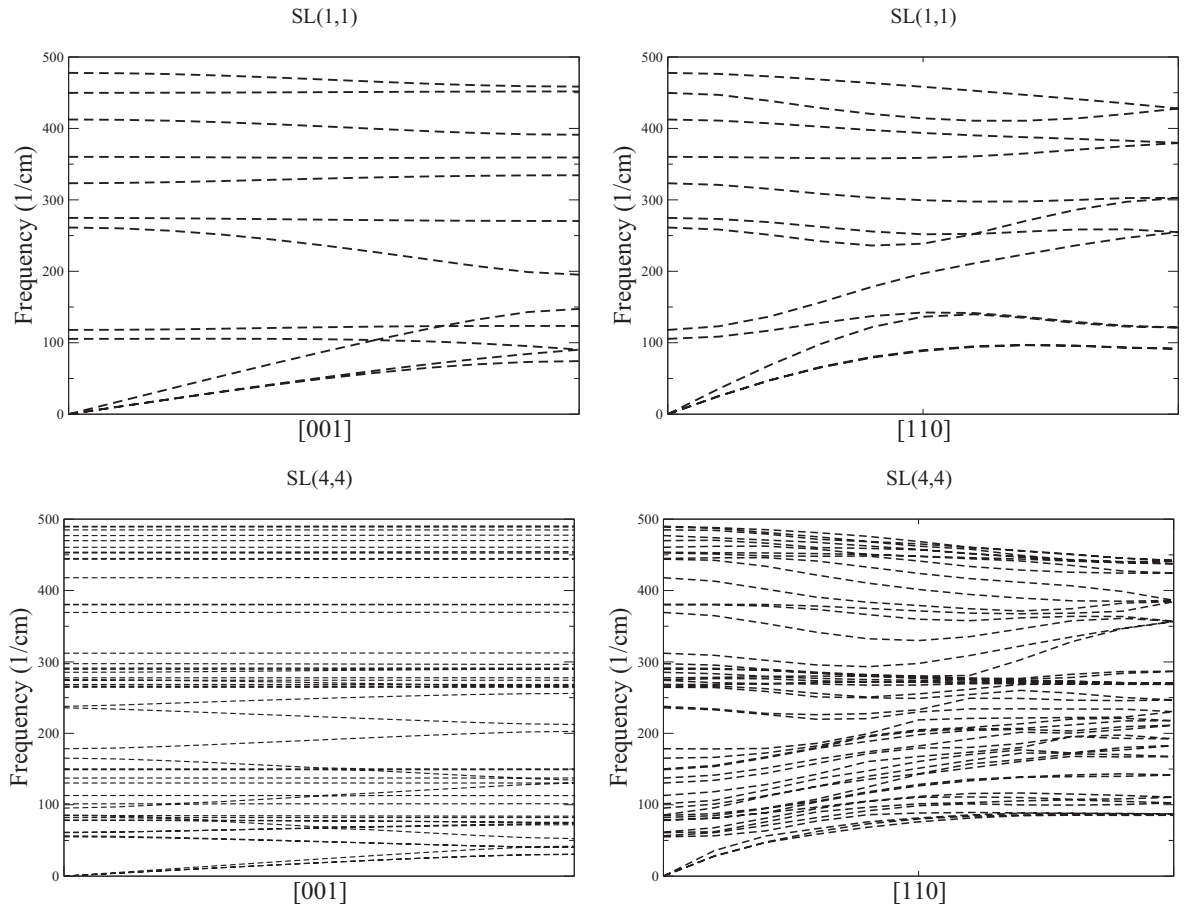

FIG. 2. Phonon dispersion curves for Si(1)Ge(1)[001] and Si(4)Ge(4)[001] superlattices. [Data for SL (1,1)[001] results originally presented in Ref. 11.]

and Slack[28]) and used a scale factor of $P = 30.0$ for point-mass-defect scattering of phonons. Use of such a scale factor was found necessary in order to ensure that the SL results at high temperature (room temperature and above) lie intermediate to the experimental "phonon-only" results for bulk Si and Ge obtained by Glassbrenner and Slack.[28] However, at temperatures lower than 100 K, the behavior deviates strongly from that of the bulk materials. It is worth remarking that for a successful match between theoretical and experimental conductivity results for bulk semiconductors, it is almost always necessary to consider much stronger point-defect scattering (hence a large-P factor). A similar observation was made in our previous work when dealing with the conductivity of a SiGe alloy sample.[10] We observe that SL (1,1) may be viewed as something like a $Si_{0.50}Ge_{0.50}$ alloy, allowing for a large concentration of point mass defects in the system. Based on these considerations, we predict that the low-temperature (below 50 K) lattice thermal conductivity component κ_{zz} of Si(1)Ge(1) would be significantly lower (by an order of magnitude) than the average of results for an equivalent bulk Si and Ge system.

We observe that our κ_{zz} results for SL (1,1) are at variance with those presented in the paper by Garg *et al.*[6] who noted that the conductivity for the thinnest superlattice period is higher than that of bulk Si and Ge. There are two possible reasons why our SL (1,1) results might be different from those presented in Ref. 6. First, Garg *et al.* performed their calculations using a fictitious superlattice structure that is made of alternating *atomic layers* of Si and Ge. Their structure bears no direct connection to the realistic SL (1,1) structure considered in our work, bearing in mind that one must consider *atomic bilayers*, not *atomic monolayers*, for superlattice structures made from Si and Ge bulk materials. Second, Garg *et al.* did not include the effects of phonon scattering from isotopic point defects and boundaries that are usually present in Si and Ge bulk materials in their calculations, which will reduce the thermal conductivity.

In Fig. 3(b), we compare two (8,8) SL calculations with parameters $P = 4.5$ and $\mathcal{P} = 0.05$ with the experimental results of Ref. 12. The boundary length was set to 100 period value ($L_B = 4.43 \times 10^{-7}$ m) as quoted in Ref. 12. We can see that we have reasonably good qualitative agreement with experimental results. The agreement is improved if we allow for some surface roughness and reduce the value of L_B to 3×10^{-7} m, around 68% of the sample size. The decrease in κ_{zz} between 200 and 300 K is a little steep (and in fact, we find that it decreases quite steeply beyond 300 K, unlike what we might expect from the results of Lee *et al.*[14]); this suggests that our best estimate of $\bar{\gamma}$ above 300 K may be a little high. However, as a first approximation, it should be sufficient, especially as the experimental behavior of this SL length is not well established for such high temperatures.

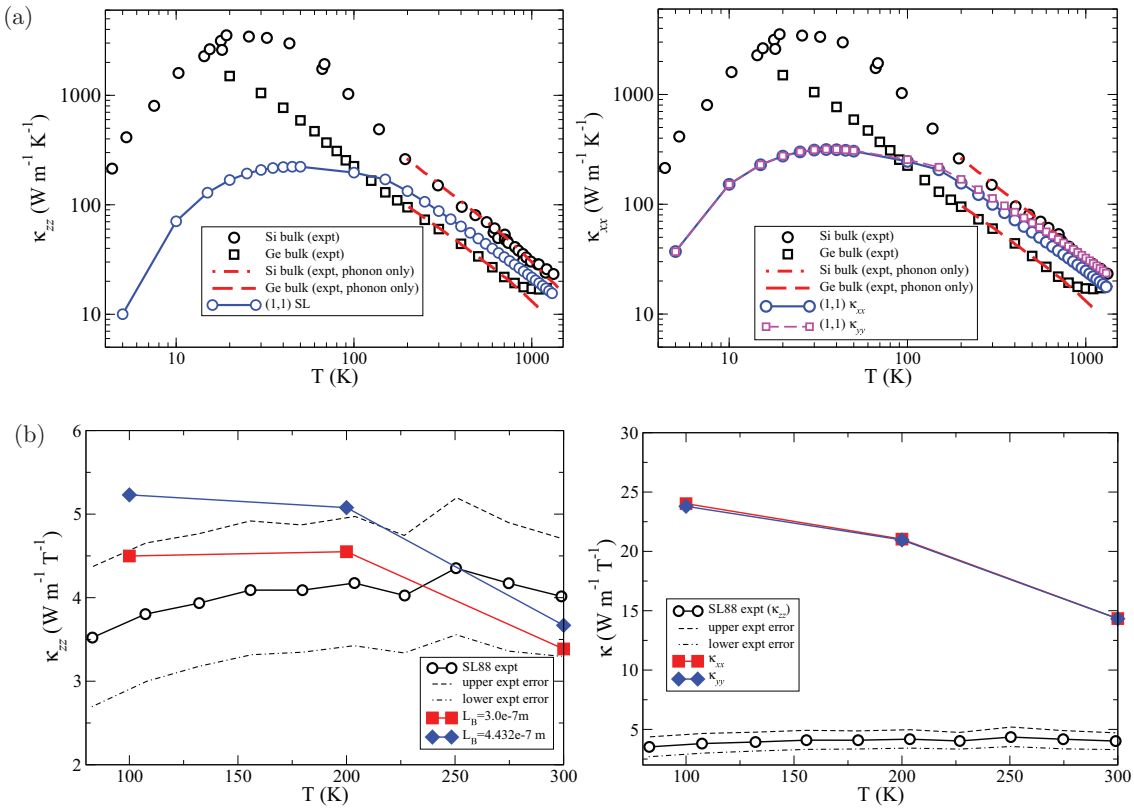

FIG. 3. (Color online) Lattice thermal conductivity tensor components (κ_{xx}, κ_{yy}, and κ_{zz}) for Si(n)Ge(n)[001] superlattice, where n represents the number of atomic bilayers. Panel (a) shows our results for the (1,1) SL together with experimental results for bulk Si and Ge read from Ref. 28. We have used the boundary length and point-mass-defect scale parameters as $L_B = 4.4 \times 10^{-3}$ mm and $P = 30.0$. Panel (b) shows our results for the (8,8) SL; the in-plane results are for the $L_B = 3.0 \times 10^{-7}$ m case. The experimental results from Ref. 12 for a sample size equivalent to 100 period value can be matched with the choice of the mass-defect scale parameter $P = 4.5$ and the interface mass-mixing probability factor $\mathcal{P} = 0.05$. The effect of reducing the L_B parameter from the 100 period value is also shown. (Experimental data in both plots in Fig. 3(a) adapted with permission from figures in Ref. 28. Copyright © American Physical Society.)

We should also caution as to the perils of taking a single experimental data set from a single sample as wholly definitive; for example, Huxtable *et al.*'s[29] measurement of a 50-Å SiGe superlattice displays a discernably lower κ_{zz} than Lee *et al.*'s[14] measurement of a SiGe SL of the same length, a discrepancy that they attribute to the use of a different growth method. We should also remark that the consideration of a smaller mass-defect scale factor of $P = 4.5$ for the (8,8) SL compared to $P = 30.0$ for the (1,1) SL is justified: whereas significantly strong atomic mixing (and thus point-mass-defect scattering) can take place for the (1,1) SL, the average amount of atomic mass mixing per period for a good quality (8,8) SL can be expected to be much smaller.

Our calculations suggest that in general κ_{zz} is lower than κ_{xx}. However, the κ_{xx} and κ_{zz} components for the (1,1) SL are not very different from each other. To explain this, we note that this system can be viewed quite similar to bulk alloy retaining nearly isotropic kappa feature. A clear difference between the in-plane conductivity components (κ_{xx} and κ_{yy}) and the growth direction component (κ_{zz}) can be noted from Fig. 3(b) for the (8,8) SL. Our calculations predict the in-plane components to be approximately 4.1–4.8 times larger than the component along the growth direction for the temperature range considered, with the anisotropy being smaller closer to $T = 300$ K. This is qualitatively similar to what is observed in Yang *et al.*'s[30] measurements of the thermal conductivity of Si(80 Å)Ge(20 Å) SLs in that the anisotropy decreases as temperature increases; however, our values of the anisotropy are smaller. The relative reduction in the κ_{zz} component is obviously due to two main factors: reduced phonon velocity and the IMS factor.

C. Trend in conductivity results with superlattice period

1. $L_B = 4.4 \times 10^{-3}$ m with and without constant IMS

In Fig. 4, we plot the n dependence of κ_{zz} for (a) systems with no IMS scattering and (b) systems with $\mathcal{P} = 0.05$ for $n > 1$. In both cases, we have considered the point-mass-defect scale factor $P = 30.0$. In general, we can see that the results with and without the inclusion of IMS are qualitatively very similar, although not quite identical. Examining the two-dimensional (2D) plots (a-i) and (b-i), we note that there exist regions below $T \lesssim 150$ for $n = 2$–4 where κ_{zz} is *greater* than the $n = 1$ result. The point at which they cross below the $n = 1$ curve moves to a lower temperature as n is increased; in the $n = 4$ case, the presence of IMS scattering moves it to a slightly lower temperature than is observed in its absence. This is most likely an effect of the replacement of the alloy

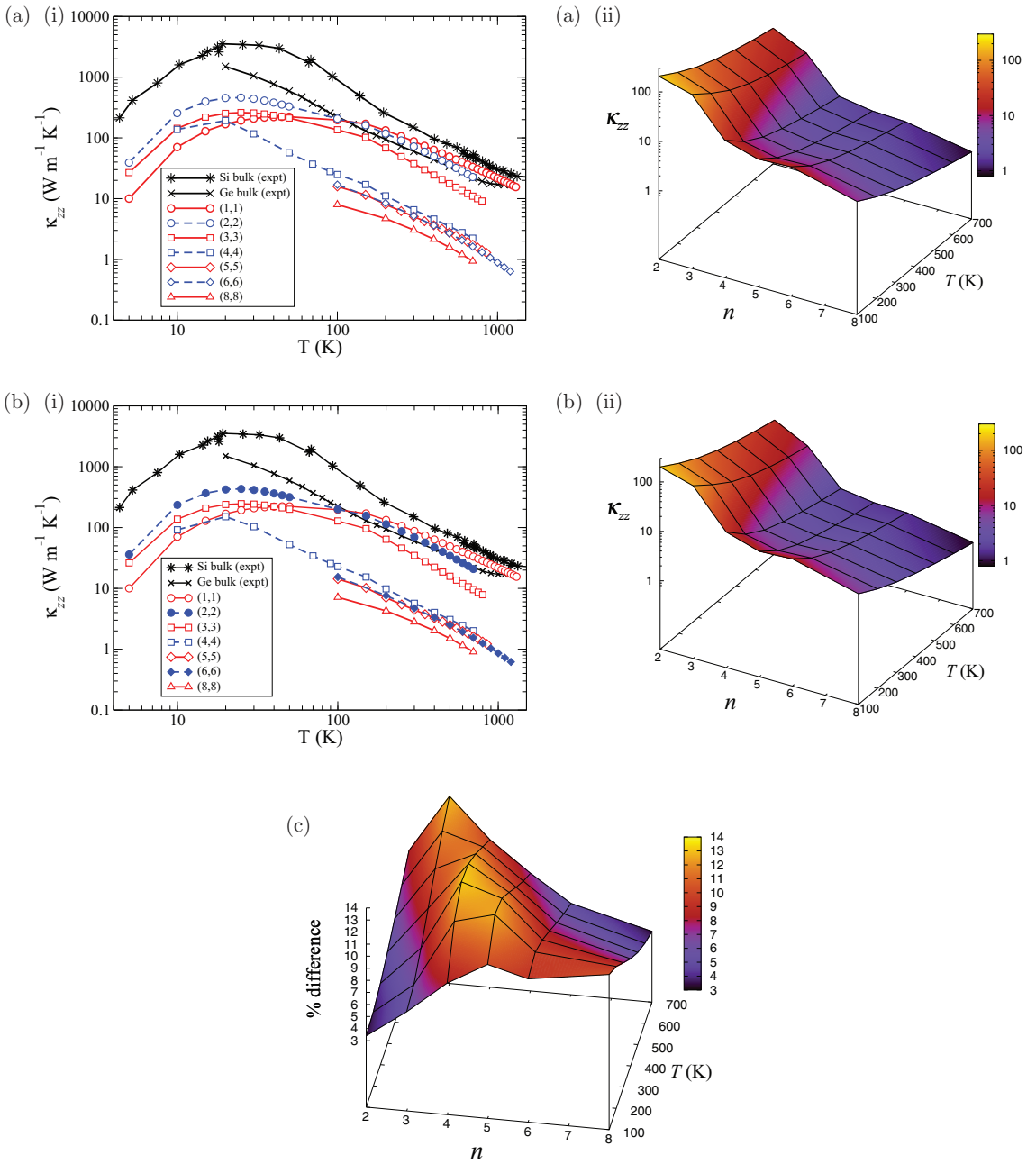

FIG. 4. (Color online) Results showing the variation of κ_{zz} with n in the $P = 30$, $L_B = 4.4 \times 10^{-3}$ m system. Panels (a) and (b) show a 2D plot (i) including experimental bulk values from Ref. 28 and a 3D plot (ii) of representative values of κ_{zz} (in units of W m^{-1} K^{-1}) between 100 and 700 K. Set (a) has $\mathcal{P} = 0$, (b) has $\mathcal{P} = 0.05$. Panel (c) shows the percentage difference in κ_{zz} due to the inclusion of IMS scattering relative to the $\mathcal{P} = 0$ results for the data points depicted in (a)(ii) and (b)(ii). (Experimental data in Figs. 4(a)(i) and 4(b)(i) adapted with permission from figures in Ref. 28. Copyright © American Physical Society.)

portion of the mass-defect contribution to scattering with the IMS contribution for $n > 1$ combined with the large value of the P parameter, entailing that the IMS scattering is not strong enough to compensate for the loss of the alloy scattering in this system. For $n \geqslant 3$, the high-temperature portions of the curves lie below the bulk experimental results; for $n = 2$ the data lie above or coincident with the Ge bulk data. One striking feature of these results is that the $n = 5$ and 6 results are almost equal; this is unexpected and we do not as yet have an explanation for it.

The three-dimensional (3D) plots in panels (a-ii) and (b-ii) are also very similar. They display points at intervals of 100 K in the range 100 to 700 K for $n = 2$–6 and $n = 8$. The general trend is for κ_{zz} to decrease as T increases (as one would expect) and also as n increases. This last decrease, however, is not simply related to n, for we begin with a rather shallow decrease between $n = 2$ and 3, which becomes more steep for $n = 3$–4, levels out and plateaus for $n = 4$–6, and has begun a further shallow descent by $n = 8$. This is not terribly consonant with experimental results, where one would expect κ_{zz} to increase

with n (at least for the sufficiently large n to which we have experimental access); this is likely in part a consequence of our using a constant $\mathcal{P}$, as we shall discuss in the following.

The plot in Fig. 4(c) describes the percentage decrease in κ_{zz} due to the inclusion of IMS scattering, and provides a clear description of the temperature region where IMS scattering is dominant in this kind of system; it runs in an approximately diagonal band from higher temperatures at $n = 2$ to lower temperatures at $n = 8$. On either side of this ridge, scattering is dominated by a different kind of process: on the left-hand

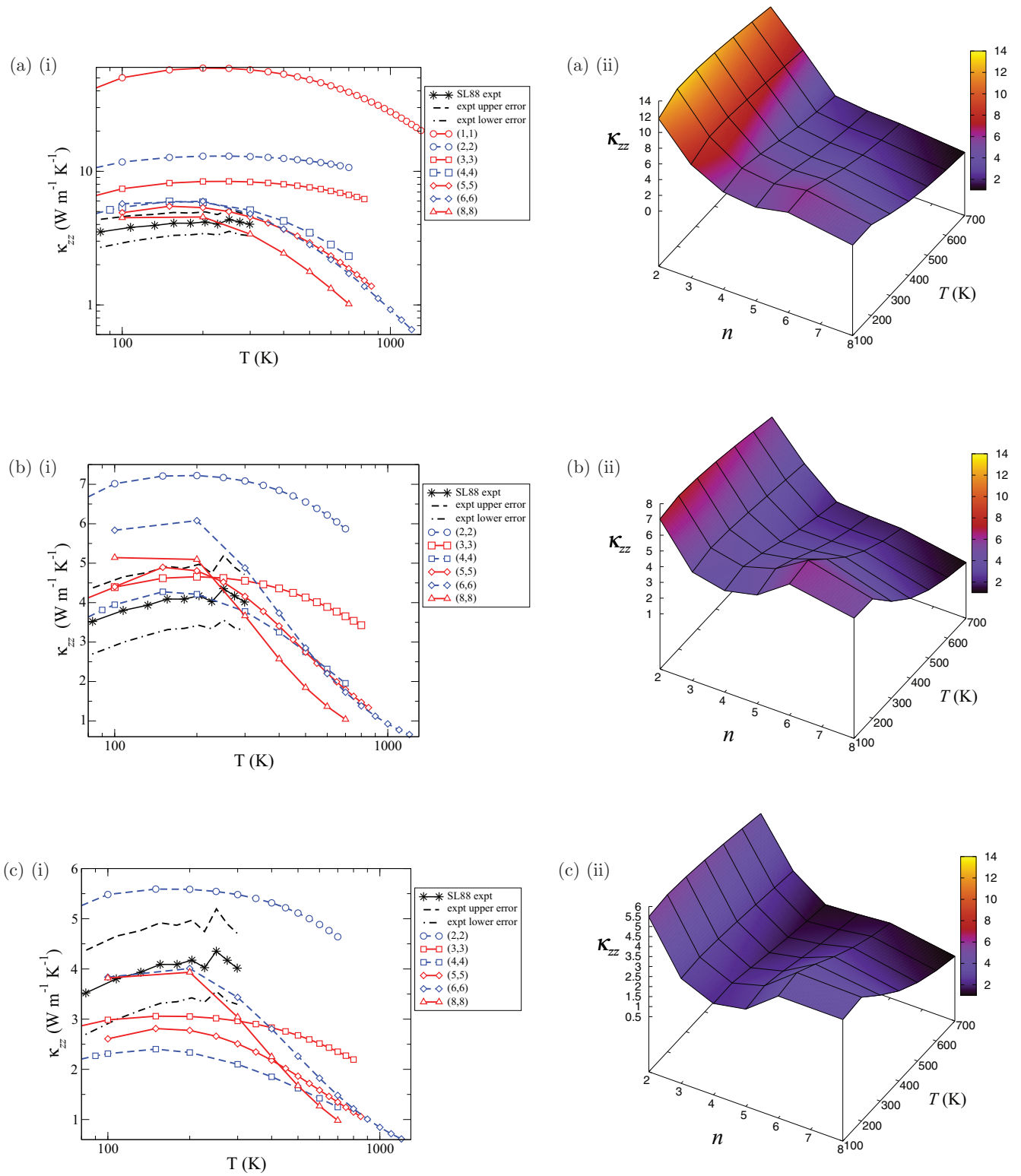

FIG. 5. (Color online) Results showing the variation of κ_{zz} with n in the $P = 4.5$, $L_B = 3.0 \times 10^{-7}$ m system. Panels (a)–(c) each show a 2D plot (i) including experimental bulk values from Ref. 12 and a 3D plot (ii) of representative values of κ_{zz} (in units of W m^{-1} K^{-1}) between 100 and 700 K. Set (a) has $\mathcal{P} = 0.05$, (b) uses $\mathcal{P}_A(n)$, and (c) uses $\mathcal{P}_B(n)$.

side (smaller n, low T), the dominant processes will be boundary scattering and mass-defect scattering, and on the right-hand side (larger n, high T), anharmonic processes will dominate. We can see that increasing n shifts the temperature at which each successive process becomes dominant downwards.

D. Consequences of varying IMS parameter with SL period index n

Keeping $\mathcal{P}$ constant would seem to contradict the experimentally observed behavior of κ_{zz} with n. But this should be unsurprising, for we have established that holding the proportion of mixing constant as n increases implies that $\mathcal{P}$ decreases. So if $\mathcal{P}$ is constant with n, this means that in order to compensate for the decrease due to the increase in n, the proportion of mixing in the bilayers adjacent to the interface must increase and/or mixing must be allowed to occur between bilayers further from the interfaces. Effectively, fixing $\mathcal{P}$ to a constant value for all n entails that as n is increased, the quality of interfaces worsens; it is no wonder that κ_{zz} might decrease with n as we see in Fig. 4!

In Fig. 5, we plot 2D and 3D plots of the behavior of κ_{zz} for (a) $\mathcal{P} = 0.05$, (b) $\mathcal{P}_A$, and (c) $\mathcal{P}_B$, (b) and (c) being defined in Eq. (11), for the $LB = 3.0 \times 10^{-7}$ m and $P = 4.5$ system which corresponds more closely to experiment than the one examined previously. First, let us examine the 2D plots in Figs. 5(a)–5(c) (i). The general trend for the $\mathcal{P} = 0.05$ case as n and T increase is generally similar to that observed for the other fixed $\mathcal{P} = 0.05$ systems in that κ_{zz} tends downwards; the exception is $n = 6$, which manages to be more or less coincident with the $n = 4$ curve near $T = 100$, but which drops to slightly below $n = 5$ at high temperatures. Examining Figs. 5(b) (i) and 5(c) (i), we see that one clear effect of increasing n consistent with the results previously discussed is that it lessens the temperature at which anharmonic effects dominate: the onset is quite rapid at $n = 8$, occurring between 200 and 300 K. We now note the following result of physical consequence, which is that the behavior of κ_{zz} with n is no longer monotonic near $T = 100$. Instead [as is also illustrated in Figs. 5(b) (ii) and 5(c) (ii)], a minimum at $n = 4$ exists beyond which κ_{zz} increases (even allowing for the $n = 8$ values being smaller in this region than the anomalous $n = 6$ ones, $n = 8$ is still larger than $n = 5$). As T increases and we move into a region where anharmonic scattering dominates, this behavior dies off and we see a restoration of the expected monotonic behavior. This lack of monotonicity for temperatures near 100 K is likely a consequence of the interaction between the effect of superlattice size on phonon behavior and the IMS scattering strength. Broadly, as n increases, the change in velocities causes κ_{zz} to decrease.[31,32] This decrease is most pronounced at small n; for larger n, κ_{zz} converges on a fixed value. Below the minimum, the decrease with n due to the velocity outweighs any effect that might arise due to the decrease in the the strength of the IMS scattering as characterized by $\mathcal{P}$; above this minimum, the effects of IMS scattering dominate, and so the decrease in $\mathcal{P}$ with n causes κ_{zz} to increase.

It would be premature to state that a global minimum at $n = 4$ would be physically observable; that would await a proper characterization of the proportion of dislocation scattering arising from the lattice mismatch of Si and Ge which is present at $n \gtrapprox 10$; such scattering might drive κ_{zz} for those n down further still. However, since dislocations are not present below that critical lattice size,[14,15] we can say that for the

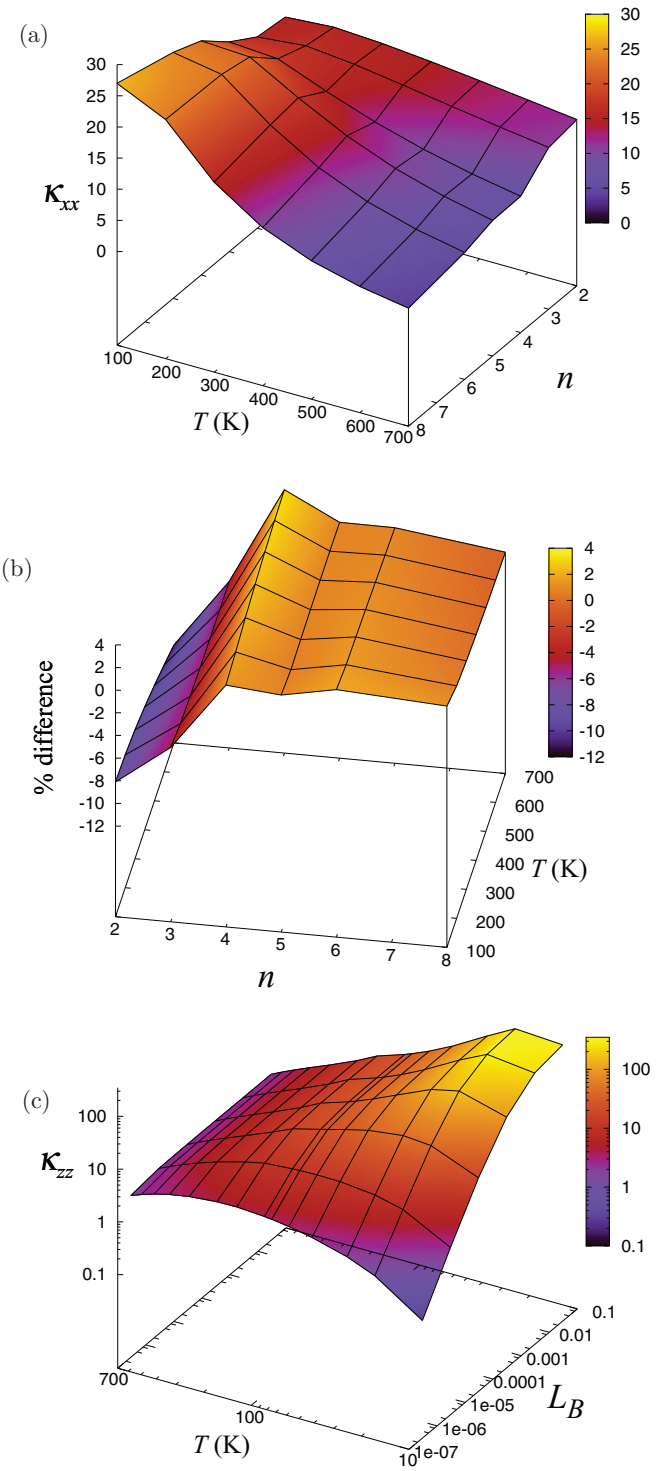

FIG. 6. (Color online) (a) Variation of κ_{xx} (in units of W m^{-1} K^{-1}) with n for the $P = 4.5$, $L_B = 3.0 \times 10^{-7}$ m system using $\mathcal{P}_A$, (b) percentage difference between κ_{xx} and κ_{yy} relative to κ_{xx} for the same system, (c) plot showing the dependency of κ_{zz} (in units of W m^{-1} K^{-1}) on L_B (in units of m) if we keep other parameters the same.

ultrathin SLs with $n \leqslant 4$, we might expect to see an increase in κ_{zz} even for fairly dirty interfaces, provided that the quality of interface is consistent between samples of different size.

In Fig. 6, we plot some other quantities of interest for a system with $P = 4.5$, $L_B = 3.0 \times 10^{-7}$ m where the IMS strength is given by $\mathcal{P}_A$. Figure 6(a) shows the behavior of κ_{xx} with T and n; here, we see that at $T = 100$ K the conductivity tends to increase with n, whereas at high temperatures it decreases with n due to the dominance of anharmonic scattering; note that there is an apparent "kink" in the behavior of κ_{xx} centered at $n = 4$. This general behavior and that κ_{xx} is much larger for a given n and T than κ_{zz} is most likely due to the absence of an interface in this direction, although one would also expect IMS scattering to have some residual effect. Figure 6(b) shows the difference between κ_{xx} and κ_{yy} expressed as a percentage of κ_{xx}. This arises as a result of the inequivalency of our chosen x and y directions as discussed in Ref. 11; as observed for the reduced conductivity in that study, we find that the difference dies off as n is increased. Figure 6(c) shows the effects of changing L_B on κ_{zz} for a (4,4) SL; the most notable is that as well as reducing the magnitude of κ_{zz} at low T, decreasing L_B also pushes the location of the maximum κ_{zz} upwards. This is important as experimental results such as those of Refs. 12 and 14 typically show a leveling off or a maximum of κ_{zz} in the region of $\gtrapprox 100$ K; this effect is probably in part a consequence of boundary scattering. This would be consistent with the experimental and numerical results of Luckyanova *et al.*[7] regarding GaAs/AlAs superlattices, where it has been shown that at temperatures of less than 300 K, surface roughness effects such as IMS mixing affect mainly high-frequency phonons; the low-frequency phonons that conduct the majority of heat remain coherent and are in fact scattered only by the boundaries.

Figure 7 displays κ_{zz} against n and T for our choices of α. The general qualitative behavior that we observed with our simple models is reproduced, and as one might expect the overall values of κ_{zz} for a given n are smaller for the $\alpha = 2.0$ case, with the (8,8) results being far below the experimental values, whereas for $\alpha = 5.0$ only the 300-K point falls outside of experimental error, and then barely (in order to obtain fully compatible results, one could reduce P slightly). One interesting difference is that the minimum κ_{zz} near $T = 100$ K for the $\alpha = 2.0$ case is no longer located at $n = 4$, but at $n = 5$,

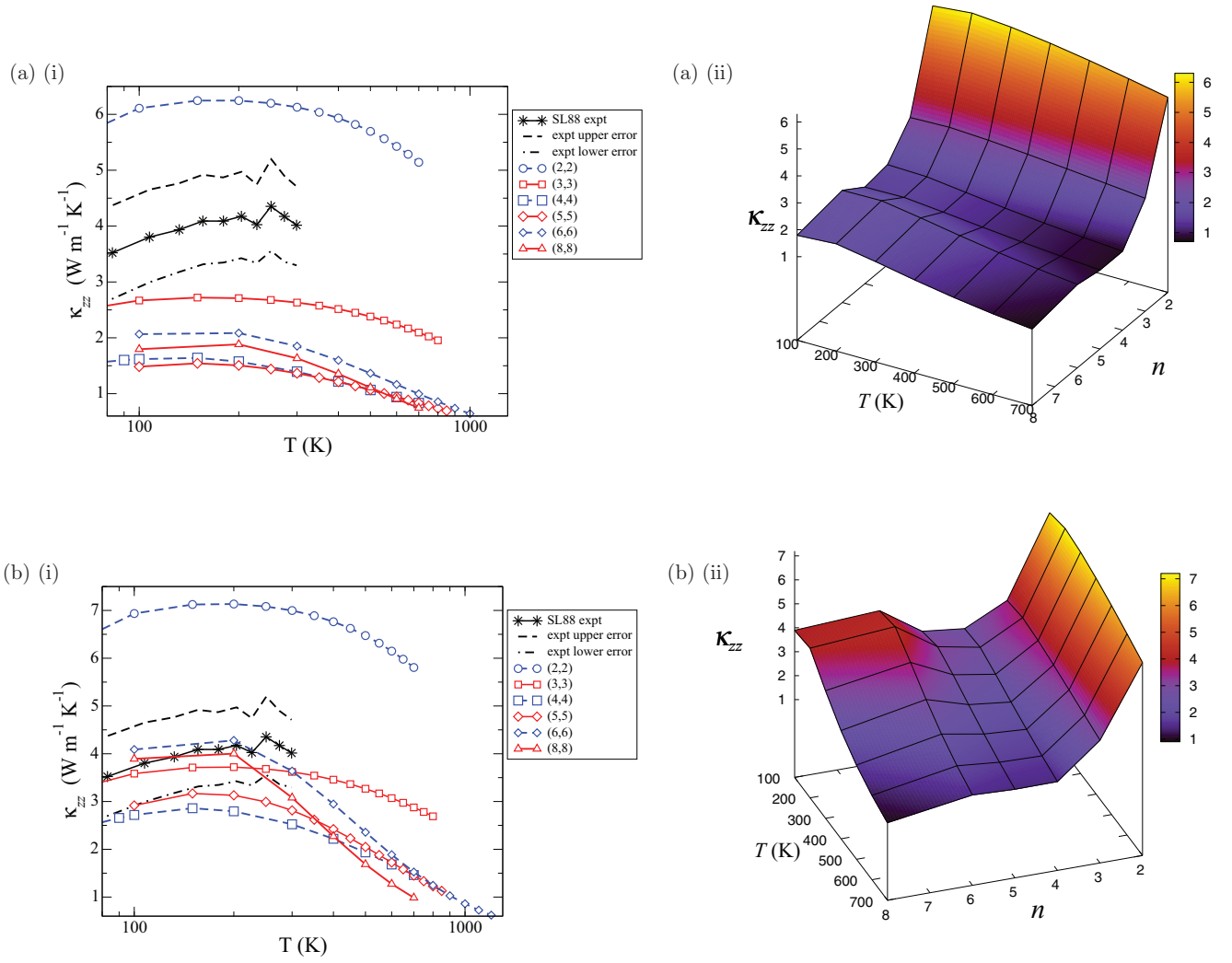

FIG. 7. (Color online) Temperature variation of κ_{zz} (in units of W m^{-1} K^{-1}) for the $P = 4.5$, $L_B = 3.0 \times 10^{-7}$ m system with $\mathcal{P}$ calculated using (a) $\alpha = 2.0$ and $B = 1.0$, (b) $\alpha = 5.0$ and $B = 1.0$ Experimental data used in the 2D plots is taken from Ref. 12.

although the difference is rather small. This suggests that the precise location of the transition from κ_{zz} decreasing as n is increased to it increasing with n will be somewhat dependent on interface quality.

The consistently anomalous (6,6) results are deserving of some discussion. It is clear from our calculations that there exist values of $\mathcal{P}(n=8) < \mathcal{P}(n=6)$ for which $\kappa_{zz}(n=8) > \kappa_{zz}(n=8)$ [for example, if we were to compare the $\mathcal{P}(n=6)$ result generated with $\alpha = 2.0$ and the $\mathcal{P}(n=8)$ result generated with $\alpha = 5.0$]. This suggests that it is possible that the models we have used do not quite capture the precise behavior of $\mathcal{P}$ with n; however, it could also be that there is some small oscillation of κ_{zz} with increasing n (even if the overall trend is upward) or that this is due to a numerical effect (such as insufficient convergence), or some combination of the three. Clarification of this issue will have to await more calculations at larger n, which are unfortunately beyond our resources at this point in time.

V. SUMMARY AND OUTLOOK

We have performed a systematic theoretical investigation of the reduction of the lattice thermal conductivity in ultrathin Si(n)Ge(n)[001] superlattices, with $1 \leqslant n \leqslant 8$, where n represents the number of atomic bilayers of a species within a repeat period. The calculations are performed using a model anharmonic Hamiltonian describing three-phonon interactions involving acoustic as well as optical phonons in a two-material superlattice structure, and an improved scheme for phonon scattering due to mass smudging at interfaces. The variation of the components with the superlattice period and sample temperature have been examined and trends extracted. The theoretical results for Si(8)Ge(8) have been successfully compared with experimental measurements for Si(22 Å)/Ge(22 Å) reported in Ref. 12. We have found that the cross-planar thermal conductivity is roughly 4.1–4.8 times smaller than the in-plane thermal conductivities for the (8,8) case for temperatures between 100 and 300 K for $\mathcal{P} = 0.05$.

We have examined in some detail the effects of various parametrizations of the IMS scattering as described by the parameter $\mathcal{P}$. Keeping $\mathcal{P}$ constant with n results in a decrease in κ_{zz} (between 3%–14% for a sample size of 4.4 mm); however, this involves making problematic assumptions regarding interface quality, which is best described by a $\mathcal{P}$ that decreases with n. Examining various models of the decay of $\mathcal{P}$ we have found that while in general the behavior of κ_{zz} at high T shows a monotonic decrease with n, at T close to 100 K we see that κ_{zz} reaches a minimum at $n = 4$–5 before beginning to increase. It is likely that this is because IMS scattering outcompetes the effect of phonon velocity that is described in Refs. 31 and 32 at larger values of n, so that the decay in $\mathcal{P}$ causes κ_{zz} to increase. Note that it can not be said that this minimum is a global one; that would depend on the effects of dislocation scattering when the lattice size exceeds $n = 10$ and is a matter beyond the scope of this study. We also observe that for the $T = 10$–100 K region, boundary scattering is the dominant effect, consistent with the findings of Ref. 7.

Since the dimensionless thermoelectric figure of merit parameter ZT is inversely proportional to the sum of the electronic and phonon contributions to the thermal conductivity, we can see that the above results have implications with respect to the thermoelectric efficiency of ultrathin superlattices, in that we should not expect the very thinnest SLs to be as thermoelectrically efficient in the cross-planar direction as slightly thicker ones in the limit where dislocation effects are unimportant; moreover, within that limit an optimal SL length where κ_{zz} is at a minimum may exist. However, the precise extent of any enhancement will be dependent upon how the electronic components of ZT change upon superlattice formation.

ACKNOWLEDGMENTS

I. O. Thomas acknowledges financial support from EPSRC (UK) Grant Award No. EP/H046690/1 which funds this work. The Intel Nehalem (i7) cluster (CERES) at the University of Exeter was used to perform the calculations in this work.

APPENDIX A: IMS SCATTERING PROBABILITY $\mathcal{P}$

As far as we are aware, there are no systematic theoretical characterizations of the degree of interface mass mixing in composite superlattice systems. In order to proceed with a theoretical discussion of IMS scattering, we must therefore devise an *ad hoc* scheme which parametrizes such mixing. We choose to characterize the strength of the IMS scattering in a given (n, n) superlattice composed of alternating multilayers A and B by the probability $\mathcal{P}$ of the interchange of a number of pairs of bilayers, one from one half of A and one from the neighboring half of B.

A description of the behavior of the IMS scattering strength with n should, in our view, possess the following desirable properties:

(i) For no value of $n > 1$ should the overall probability of the interchange of a number of bilayers $\mathcal{P}$ exceed 0.5.

(ii) The probability of the interchange of a given bilayer with another should *decrease* with the distance separating the two bilayers.

(iii) As n becomes very large and the system becomes bulklike, $\mathcal{P}$ should tend towards 0 as IMS scattering should become negligible.

In order that $\mathcal{P}$ can be properly defined, we shall label each bilayer in the SL sequentially as $l = 1, \ldots, N_{\mathrm{MAX}} = 2n$, and also those bilayers in section A of the SL sequentially as $k = 1, \ldots, n$. Let us define the probability that a bilayer labeled k will interchange itself with a bilayer labeled k as

$$\mathbb{P}^{kl}_{\mathrm{SWAP}} = \frac{1}{N_{\mathrm{MAX}}(|k-l|-1+B)^{\alpha}}, \tag{A1}$$

where $k \neq l$, and the subtraction of 1 in the denominator arises so that a pair at the interface (or an adjacent pair) will have $\mathbb{P}^{kl}_{\mathrm{SWAP}} = \frac{1}{N_{\mathrm{MAX}} B^{\alpha}}$. The normalizing factor N_{MAX} arises from a requirement that if $\alpha = 0$, the sum of the probabilities of there being a swap *and* the probability of their being no swap for a given k are equal, in accordance with the principle of indifference, i.e.,

$$\sum_{l,\, l \neq k} \mathbb{P}^{kl}_{\mathrm{SWAP}} + P^{k}_{\mathrm{NO\ SWAP}} = 1. \tag{A2}$$

This allows us to say that B^{α} controls the deviation of $\mathbb{P}^{kl}_{\mathrm{SWAP}}$ at the interface from what we would "expect" given

that principle; if $B^\alpha > 1$, mixing at the interface or between adjacent pairs is less likely, if $B^\alpha < 1$ it is more likely. α controls how quickly the probability of mixing decays with distance. Note that if $B > 1$ it is important to check that the probability distribution satisfies Eq. (A2) and that $P^k_{\text{NO SWAP}}$ has a reasonable value.

A modification must be made to $\mathbb{P}^{kl}_{\text{SWAP}}$ for the purposes of our calculations so as to include periodicity. In that case, we must also account for swaps between bilayers in neighboring cells and bilayers in the cell of interest. We may do this by modifying the expression for $\mathbb{P}^{kl}_{\text{SWAP}}$ as follows:

$$\mathbb{P}^{kl}_{\text{SWAP}} = \frac{1}{2N_{\text{MAX}}} \sum_i^2 \frac{1}{(||k-l| - G_i| - 1 + B)^\alpha}, \tag{A3}$$

where $G_1 = 0$ and $G_2 = N_{\text{MAX}}$. We are interested in bilayer exchanges that have some physical effect on the behavior of the system, that is, where a bilayer labeled k has an exchange with a bilayer $l \notin \{k\}$ (that is, a bilayer in A exchanges with a bilayer in B). For such exchanges, we define an overall probability for each k:

$$\mathbb{P}^k_{\text{SWAP}} = \sum_{l \notin \{k\}}^{N_{\text{MAX}}} \mathbb{P}^{kl}_{\text{SWAP}}. \tag{A4}$$

We are ultimately interested in $\mathcal{P}$, the overall probability of there being some number of interchanges, which will give us an estimate of the strength of IMS scattering. This is easy enough to calculate. First, we calculate the probability that a given bilayer k will *not* exchange with a bilayer in B:

$$\mathbb{P}^k_{\text{NO SWAP}} = 1 - \mathbb{P}^k_{\text{SWAP}}. \tag{A5}$$

Next, we calculate the probability that no bilayers whatsoever are exchanged between A and B:

$$\mathbb{P}_{\text{NO SWAP}} = \prod_{k=1}^{n} \mathbb{P}^k_{\text{NO SWAP}}. \tag{A6}$$

It then follows that

$$\mathcal{P} = 1 - \mathbb{P}_{\text{NO SWAP}}. \tag{A7}$$

For the correct choices of B and α, this satisfies the first and third conditions.

APPENDIX B: ANHARMONIC INTERACTION TERM

We shall begin with the following expression for the third-order perturbative term in the elastic continuum potential, suitable for a single (bulk) material

$$\mathcal{V}_3 = \bar{\gamma}\sqrt{\frac{\hbar^3}{2\rho N_0 \Gamma}} \sum_{\substack{qs,\, q's',\\ q''s''}} \frac{\mathcal{B}_{qs,\, q's',\, q''s''}}{\sqrt{\omega(qs)\omega(q's')\omega(q''s'')}} \delta_{q+q'+q'',\, G} \times (a^\dagger_{qs} - a_{-qs})(a^\dagger_{-q's'} - a_{q's'})(a^\dagger_{q''s''} - a_{-q's'}), \tag{B1}$$

with $a^\dagger_{qs}$ (a_{qs}) being the phonon creation (annihilation) operator for a given mode qs, ρ being mass density, and c_s being the speed of a phonon belonging to branch s. In Ref. 10, we expressed the term $\mathcal{B}$ as

$$\mathcal{B}_{i,j,k} = [\sqrt{\omega(i)\omega(j)}[\omega(i) + \omega(j)]|\omega_\Gamma(k) - \omega(k)|/c(k) + \text{similar terms with } i,\ j,\ \text{and } k \text{ interchanged}]/3!, \tag{B2}$$

where i, j, k label phonon modes, and $c(k)$ is the *momentum-dependent*, i.e., phase speed for the mode k. We take this opportunity to assert that in the spirit of the continuum scheme $c(k)$ should be considered as the phase speed in the long-wavelength acoustic limit, i.e., for acoustic phonon wave vectors close to zero. We thus replace $c(k)$ with a branch-average speed $\bar{c}$ obtained from the acoustic branches in the long-wavelength limit (the q point closest to Γ), and replace $\mathcal{B}$ with $\mathcal{B}^{\text{modified}}$ as

$$\mathcal{B}^{\text{modified}}_{i,j,k} = [\sqrt{\omega(i)\omega(j)}[\omega(i) + \omega(j)]|\omega_\Gamma(k) - \omega(k)| + \text{similar terms with } i,\ j,\ \text{and } k \text{ interchanged}]/(6\bar{c}). \tag{B3}$$

For a composite material system, such as a superlattice, the third-order force constants implicitly included in Eq. (B1) should be modified to account for two new features:[20] (i) the presence of more than one material species, and (ii) additional reciprocal translation vectors resulting from superlattice periodicity. Following Ren and Dow[20] and some lengthy algebraic steps, the application of Fermi's golden rule results in the expression for phonon anharmonic relaxation rate as presented in Sec. II C of this paper.

[1] G. Chen, M. S. Dresselhaus, G. Dresselhaus, J.-P. Fleurial, and T. Caillat, Int. Mater. Rev. **48**, 45 (2003).
[2] J.-C. Zheng, Front. Phys. China **3**, 269 (2008).
[3] G. P. Srivastava, *The Physics of Phonons* (Taylor & Francis, New York, 1990).
[4] M. G. Holland, Phys. Rev. **132**, 2461 (1963).
[5] N. Mingo, D. A. Stewart, D. A. Broido, and D. Srivastava, Phys. Rev. B **77**, 033418 (2008).
[6] J. Garg, N. Bonini, and N. Marzari, Nano Lett. **11**, 5135 (2011).
[7] M. N. Luckyanova, J. Garg, K. Esfarjani, A. Jandl, M. T. Bulsara, A. J. Schmidt, A. J. Minnich, S. Chen, M. S. Dresselhaus, Z. Ren, E. A. Fitzgerald, and G. Chen, Science **338**, 936 (2012).
[8] S. P. Hepplestone and G. P. Srivastava, Phys. Rev. B **82**, 144303 (2010).
[9] S. P. Hepplestone and G. P. Srivastava, Phys. Rev. B **84**, 115326 (2011).
[10] I. O. Thomas and G. P. Srivastava, Phys. Rev. B **86**, 045205 (2012).
[11] I. O. Thomas and G. P. Srivastava, Phys. Rev. B **87**, 085410 (2013).
[12] T. Borca-Tascuic, W. Liu, T. Zeng, D. W. Song, C. D. Moore, G. Chen, K. L. Wang, M. S. Goorsky, T. Radetic, R. Gronsky, T. Koga, and M. S. Dresselhaus, Superlattices Microstruct. **28**, 199 (2000).
[13] P. Carruthers, Rev. Mod. Phys. **32**, 92 (1961).
[14] S.-M. Lee, D. A. Cahill, and R. Venkatasubramanian, Appl. Phys. Lett. **70**, 2957 (1997).
[15] Y.-W. Mo, D. E. Savage, B. S. Swartzentruber, and M. G. Lagally, Phys. Rev. Lett. **65**, 1020 (1990); T. Ma, H. Tu, B. Shao,

A. Liu, and G. Hu, Mater. Sci. Semicond. Process. **9**, 49 (2006).
[16]J. M. Ziman, *Electrons and Phonons* (Oxford University Press, New York, 1967).
[17]G. P. Srivastava, Philos. Mag. **34**, 795 (1976).
[18]P. G. Klemens, in *Solid State Physics*, edited by F. Seitz and D. Turnbull (Academic, New York, 1958), Vol. 7, p. 1.
[19]B. K. Ridley and R. Gupta, Phys. Rev. B **43**, 4939 (1991).
[20]S. Y. Ren and J. D. Dow, Phys. Rev. B **25**, 3750 (1982).
[21]P. Gianozzi, S. Baroni, N. Bonini, M. Calandra, R. Car, C. Cavazzoni, D. Ceresoli, G. L. Chiarotti, M. Cococcioni, I. Dabo, A. Dal Corso, S. de Gioroncoli, S. Fabris, G. Fratesi, R. Gebauer, U. Gerstmann, C. Gougoussis, A. Kokalj, M. Lazzeri, L. Martin-Samos, N. Marzari, F. Mauri, R. Mazzarello, S. Paolini, A. Pasquarello, L. Paulatto, C. Sbraccia, S. Scandolo, G. Sclauzero, A. P. Seitsonen, A. Smogunov, P. Umari, and R. M. Wentzcovitch, J. Phys.: Condens. Matter **21**, 395502 (2009); code available from http://www.quantum-espresso.org.
[22]These being the pseudopotentials Si.pz-vbc.UPF and Ge.pz-bhs.UPF, available from http://www.quantum-espresso.org.
[23]H. J. Monkhorst and J. D. Pack, Phys. Rev. B **13**, 5188 (1976).
[24]W. B. Daniels, Phys. Rev. Lett. **8**, 3 (1962).
[25]W. B. Gauster, J. Appl. Phys. **44**, 1089 (1973).
[26]B. Yates, *Thermal Expansion* (Plenum, New York, 1972).
[27]E. S. Landry and A. J. H. McGaughey, Phys. Rev. B **79**, 075316 (2009).
[28]C. J. Glassbrenner and G. A. Slack, Phys. Rev. **134**, A1058 (1964).
[29]S. T. Huxtable, A. R. Abramson, A. Majumdar, A. Shakouri, E. T. Croke, and C. C. Ahn, in *2002 ASME International Mechanical Engineering Congress and Exposition: Microelectromechanical Systems, IMECE 2002-39239, 17–22 November 2002, New Orleans, LA* (ASME, New York, 2002), pp. 19–23.
[30]B. Yang, W. L. Liu, J. L. Liu, K. L. Wang, and G. Chen, Appl. Phys. Lett. **81**, 3588 (2002).
[31]P. Hyldgaard and G. D. Mahan, Phys. Rev. B **56**, 10754 (1997).
[32]S. Tamura, Y. Tanaka, and H. J. Maris, Phys. Rev. B **60**, 2627 (1999).